Prod. Eng. Res. Devel. (2017) 11:389–399
DOI 10.1007/s11740-017-0746-3

PRODUCTION PROCESS

Experimental and computational appraisal of the shape accuracy of a thin-walled virole aero-engine casing manufactured by means of laser metal deposition

Loucas Papadakis[1] · **Carl Hauser**[2]

Received: 18 January 2017 / Accepted: 30 May 2017 / Published online: 6 June 2017

Abstract Laser metal deposition (LMD) of metallic powders, especially of high-strength nickel based alloys, allows for the manufacturing of components of high shape complexity and load capacity. However, high temperature gradients, induced during laser processing may have an impact on the product quality, especially when it comes to the geometrical accuracy of thin-walled components. This paper aims to provide a modelling approach of the heat effects during LMD manufacturing of a thin-walled virole aero-engine structure, in order to calculate possible shape deviations compared to the target CAD geometry. Hereby, a model reduction method is facilitated which allows the finite element analysis of such larger components in reasonable time. Major process characteristics as heat input, molten region geometry, material deposition (i.e. layer thickness), temperature dependent material and powder properties, phase transformation, process sequence and convection effects are taken into account. The proposed model aims to decrease time consuming trial-and-error testing effort during process design and development by providing reliable results on the shape accuracy of components. The computed final shape of the final product was compared to 3D measurements on a real demonstrator virole component.

✉ Loucas Papadakis
l.papadakis@frederick.ac.cy

Carl Hauser
carl.hauser@twi.co.uk

[1] Department of Mechanical Engineering, Frederick University, Y. Frederickou Str. 7, 1036 Nicosia, Cyprus

[2] TWI Technology Centre Yorkshire, Advanced Manufacturing Park, Wallis Way, Catcliffe, Rotherham S60 5TZ, UK

Keywords Additive manufacturing · Laser metal deposition/powder · Finite element analysis · Shape accuracy

1 Introduction

1.1 Background

Laser metal deposition (LMD) is an additive layer manufacturing (ALM) process utilised to fabricate and repair three-dimensional components by deposing metallic powder or wire through their melting and re-solidification with the aid of layer-wise paths as defined by a CAD model [1–3]. Due to the narrow heat input during the laser deposition process thin-walled geometries can be achieved [4]. This, in combination with relatively high laser transverse speed creates a severe temperature cycle and high temperature gradients across the processed layers. As a result, shrinkage of the built-up geometry is to be expected which induces an unexpected shape deformation, especially when removing parts from their substrate. LMD offers certain advantages in modern manufacturing industries such as system flexibility, direct from CAD manufacture, just in time and the ability to produce components of high density [2]. Additionally, LMD has flexibility to process different metal powders (aluminium alloys, nickel based steel alloys and titanium based alloys), giving application in a wide range of industrial sectors, e.g. aerospace and aero-engine manufacturing [5, 6].

In spite of the considerable advantages, LMD also exhibits process deficits. Based on the so-called temperature gradient mechanism (TGM), thermal stresses are induced and, depending on the plasticization behaviour of the material, stresses remain (i.e. residual stresses) in the

component after process completion and during cooling to ambient temperature [7, 8]. The formation of residual stresses is directly connected with the final component deformation. Additionally, extensive stresses during processing can lead to cracks which affect the final quality of the built-up product [9].

The rising potentials of the LMD processes motivates industry and research to develop simulation techniques for accompanying the production process and predict structural characteristics in advance so as to streamline the design for experimentation during process development. Several studies already exist in the literature in which the process and material behaviour during LMD processing are investigated. Moreover, the selection and control of suitable process parameters is performed in order to achieve process feasibility [10–12]. Hereby, manufactured part densities are achieved exceeding 99% of the theoretical densities. The most important process parameters for achieving a high quality fusing of the powder particles or wire during LMD processing are: the powder or wire material and the laser beam type, the laser power, the laser feed speed and the layer thickness. Additionally, further process effects such as the weld pool width, depth and length as well as the deposition sequence and the overall part shape influence the final shape accuracy and residual stresses development [13, 14]. It is observed that a combination of the heat input and consequently the temperature gradient mechanism which determines the molten pool characteristics together with the part geometry and post-treatment operations, i.e. cutting, are decisive for the occurrence of shape distortions [15].

1.2 Motivation

The motivation of this paper arises from the recent high potential of the metallic layer advanced manufacturing technologies for the production of complex aero-engine components and the need to integrate suitable, time efficient and reliable simulation methods in the process design phase [16, 17]. Along with the established manufacturing processes, appropriate modelling strategies have to be evaluated with respect to the various non-linear physical effects occurring in the structure during LMD.

The outcome of this contribution is a modelling method which demonstrates the potentials of modelling and simulation of the heat effects of the LMD processes in predicting the shape distortion of industrial relevant applications. The findings of this method should enable process and product developers to fabricate high quality components by reducing time intensive trial-and-error during process design. To this end, the proposed modelling method is evaluated with the aid of a real large aero-engine thin-walled combustor casing structure. This will enable the demonstration of the potentials of the finite element analysis of larger components with reasonable computational effort in terms of their shape accuracy. First, a transient thermal model of powder deposition during LMD is implemented in a layer-wise approach [8, 15]. Hereby, the heat input was selected in such a way so that the bond, i.e. penetration, of the current processed layer into the underlying layer was provided. Thereafter, based on the process heat input a transient thermo-mechanical simulation was performed in order to calculate the stresses and the component's deformation. Finally, a post-treatment operation, i.e. the virole part removal from the base plate, is performed in order to concur with the manufacture of the real demonstrator virole component.

Table 1 indicates the focus of the presented application example considering particular additive manufacturing process effects and the involved new simulation challenges as identified in this work.

2 LMD process parameters

2.1 Virole demonstrator component

In LMD, a weld track is formed using metal powder or wire as a filler material which is fed, through a nozzle, to a melt pool created by a focused high power-density laser beam (high power CO_2 or fibre laser). For the powder, an inert gas carrier transports and focuses the powder into a small area in the vicinity of the laser beam focus (powder-gas beam focus). By traversing both the nozzle and laser, a new material layer develops with precise accuracy and user-defined properties. The application of multi-layering

Table 1 Focus of the application example in terms of the shape accuracy modelling of the LMD/powder manufacturing process

Application example	Manufacturing process effects	Simulation challenges
Rotational symmetric thin-walled aero-engine combustor casing (Fig. 2)	Powder deposition Laser beam powder melting Binding of deposited powder with underlying solidified material Cut-off from substrate and spring-back of final built-up component	Analysis of large thin-walled component Facilitation of symmetry conditions Consideration of cut-off operation and of spring-back effect Evaluation of model results with the aid of 3D scans

techniques allows 3D structures to be created as illustrated schematically in Fig. 1, whereas parts manufactured by LMD tend to approximate the CAD shape.

The virole demonstrator combustor casing was an axis-symmetric cylindrical ring with a maximum diameter of 300 mm as presented in Fig. 2. The wall thickness was 0.8 mm throughout and the part was 88.0 mm high. Such components are generally produced by forming and welding metal sheets together. The estimated cost for the manufacture of a prototype is €50,000 with a lead time of 6–9 months taking into account the need to design and manufacture of tooling. Hence, by utilising the proposed laser metal deposition technique the focus was to assess suitability for prototype testing purposes. The material was an Inconel alloy IN718 and the final LMD part required an overall density greater than 99% in relation to the wrought alloy. The porosity requirements during a metallographic analysis were set to be less than 0.1 mm and no thermal stress cracking should be present. The surface quality should not exceed 25 µm of average roughness (Ra). Particularly, the main objective of this prototype manufacture was to obtain high quality dimensional accuracy compared to ideal CAD geometry.

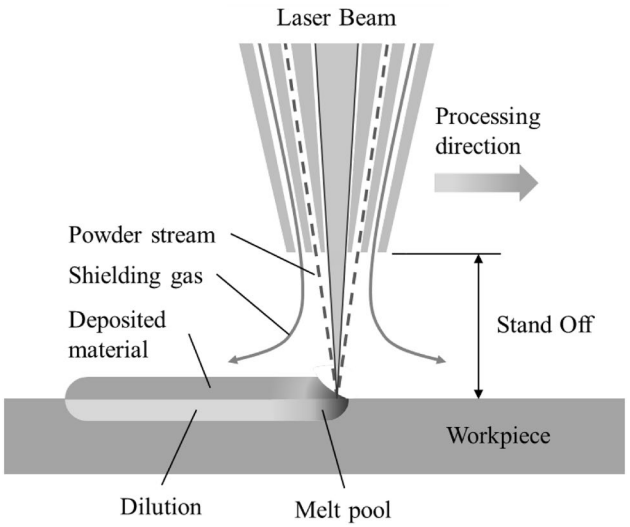

Fig. 1 Schematic illustration of the laser metal deposition process with powder (LMD/p)

2.2 Process performance and parameters

The manufacturing work was carried out at TWI, UK using a Trumpf DMD505 laser deposition system. This system comprised of; (1) A Trumpf 1.8 kW HQ CO_2 laser, a 5-axis single cantilever Cartesian gantry system with a processing envelope of 2 m (x-axis) × 1.1 m (y-axis) × 0.75 m (z-axis), (2) a Nikken 5AX-400ZA 2 axis CNC positioning table (rotation and tilt capability), (3) a Sinumerik 840D Siemens controller (capable of controlling all seven axes) and (4) a Sulzer Metco dual hopper 10-C powder feeder with 1.5 L capacity per hopper and a temperature controlled heating jacket. The cladding nozzle was a 50 mm coaxial powder feed nozzle supplied by Fraunhofer ILT, Germany. Argon gas, supplied from a BOC Cryocyl tank and distributed through a Cryospeed system, was used for 'through the nozzle' work piece shielding and for the powder carrier gas. During the work, TWI developed its own CAM software for the generation of a 3 + 2 axis toolpath direct from CAD data for the manipulation of the nozzle

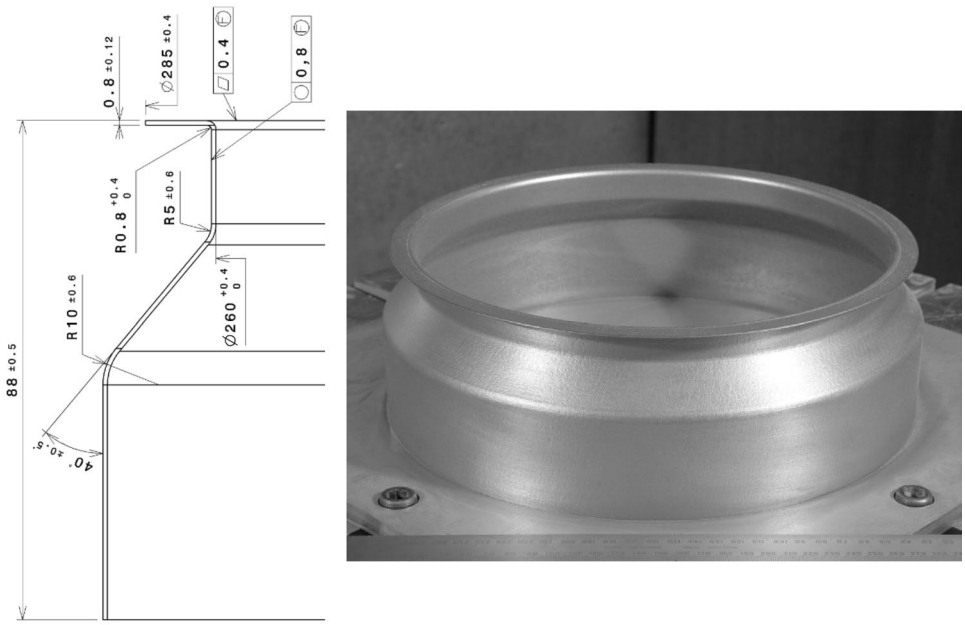

Fig. 2 Real demonstrator and sectioned CAD file of the virole combustor casing with a maximum diameter of 300 mm

Table 2 Process parameters of LMD/p with IN718 powder for the virole casing manufacture

Process parameters	Value/units
Laser power	925 W
Scan speed	1200 mm/min
Laser beam focus diameter	0.85 mm
Argon shielding gas (1.0 bar)	3.0 L/min
Increment per revolution in building direction (layer thickness)	0.18 mm
Powder feed rate	2.5 g/min
Argon gas for powder feed (1.5 bar)	3.4 L/min
Powder-gas focus diameter	0.5 mm

(*x,y,z*-axes) and CNC table (rotation and tilt). For this work the laser power was in range 850–950 W, scan speed in range 1000–1200 mm/min and a layer thickness in range 0.18–0.22 mm. Table 2 summarises the process parameters of the LMD process with IN718 powder.

3 Modelling of LMD/p manufacture of the thin-walled virole casing

3.1 Model reduction considerations

Different numerical approaches were proposed in previous studies which account for the numerous physical effects within the manufacturing process of additive manufacturing processes, especially LMD [16, 17]. The authors proposed in previous work a modelling reduction approach for replicating the heat input during the build-up process with metallic powders for practical industrial applications. Initially, detailed models of a moving heat source replicating the laser beam and the transient development of the molten pool during scanning were investigated for SLM enabling the computational reproduction of real macrographs. Thereafter, a temperature profile on whole lengths of scan vectors representing the total heat input per unit length was proposed. Based on this simplification strategy, a temperature profile in whole layers or multi layers, so-called global model, representing the total heat input per area or volume was applied for industrial relevant examples [15].

The proposed model reduction was applied due to the extended computing capacity and duration when modelling the transient circular motion for the whole structural geometry. Contrary to more detailed transient heat source models which consider the exact scanning path, the aim of the reduced models is to substitute the deposition path of each layer by areas or volumes with an equivalent heat quantity as thermal load. Therefore, based on this reduction approach it is possible to calculate the residual stresses and deformations of complete parts. A global approach for the modelling of 3D components contains all the occurring transient physical effects during deposition processing, e.g. temperature gradients, melting and solidification, convection and cooling effects, material phase transformation and material properties change, whereas solely the transient deposition path for each layer is substituted with an equivalent thermal load over a coarser, i.e. 'thicker', model layer.

In case of modelling of the introduced virole structure a reduction approach as investigated in previous studies was adopted. Compared to the SLM processing LMD differs in terms of scan speed (slower process) and cooling factors. The difference in cooling comes from the fact that whilst components manufactured by SLM are embedded in powder until the process is completed, an LMD manufactured component is exposed in the air. For this reason a convection heat transfer coefficient was defined similarly to convectional welding processes ($\alpha = 25$ W/m^{2}K) as defined in past modelling works of the welding heat effects [18]. Taking advantage of the symmetry of the component and the fact that the continuous helicoid LMD processing of the laser does not create any significant asymmetry, as this was proved by 3D measurements on the virole geometry in axial and radial direction with marginal variation to be presented in the following sections, a quarter of the virole component was modelled, as shown in Fig. 3.

3.2 Process performance and parameters

A simultaneous equivalent heat input for the whole length of four (4) layer thicknesses (equal to 0.72 mm) was defined in the FE model of the virole part as an average time function of temperature. The temperature function was selected in such a manner so that sufficient penetration of the melt in the underlying layer is provided as shown in Fig. 4. The temperature change as a function

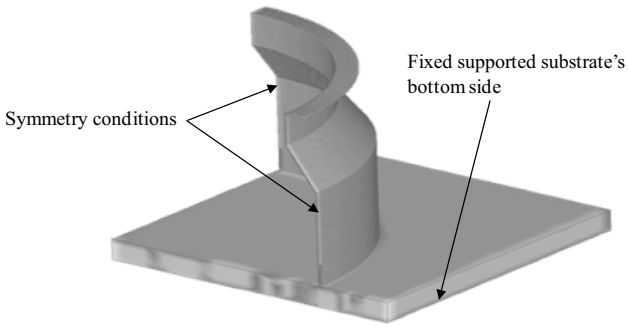

Fig. 3 Quarter model of the virole demonstrator component

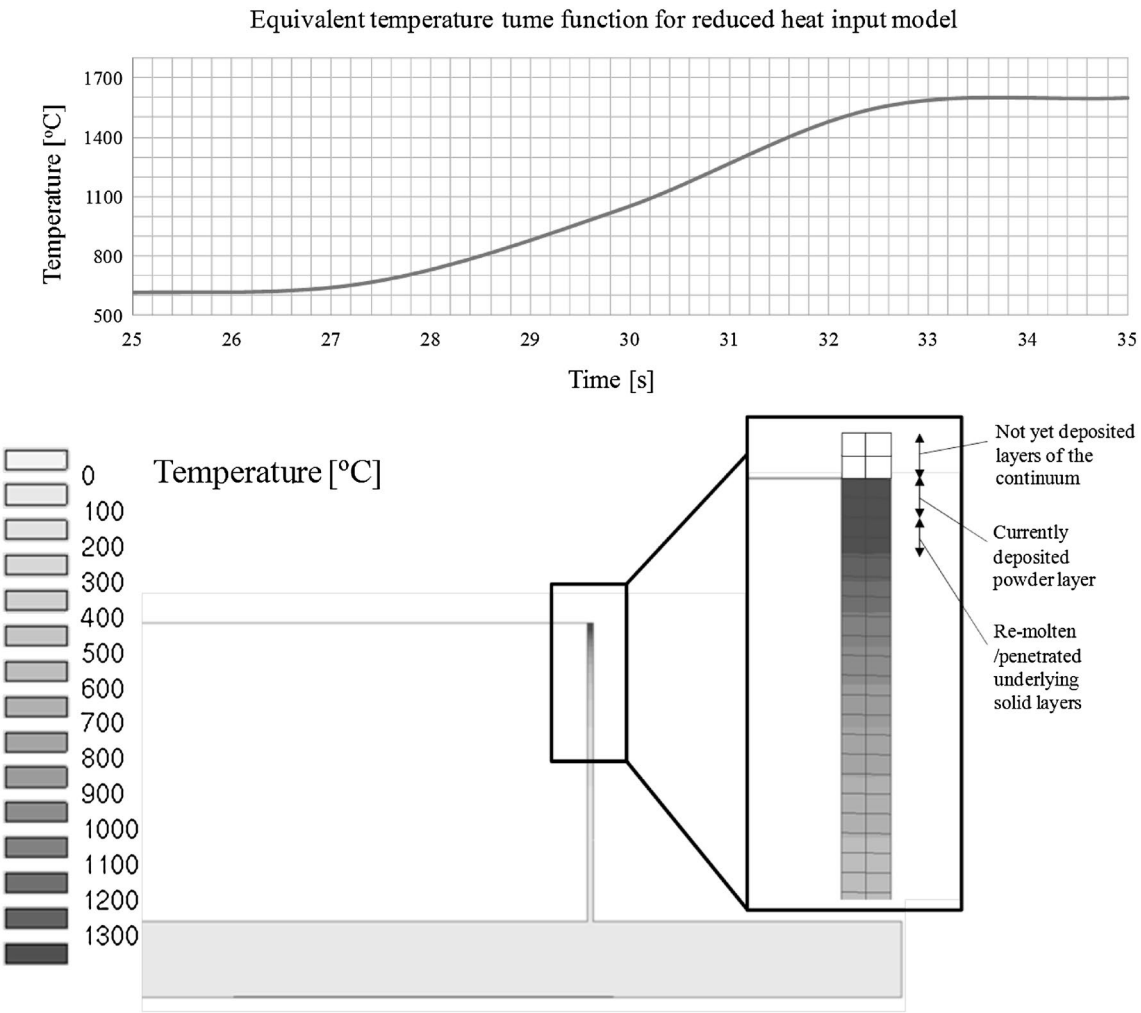

Fig. 4 Transient temperature field along the virole part depth indicating the molten model layer and penetrated underlying solid for the equivalent heat input temperature function

of time was obtained through the lumped capacitance method based on the rate of input energy in Watt, the heat transfer coefficient, the surface area and the volume of the layers, the specific heat capacity and the density of the powder. After the heat input on each processed layer a 30 s time period for cooling was foreseen in the simulation for the time taken for the laser to reach the beginning of the quarter model during the deposition process until the thermal loading of the new layer commences. The built-up process of the model during powder deposition in a layerwise modelling approach and the respective transient thermal calculation is demonstrated in Fig. 5.

4 Shape distortion computational results

The thermal analysis presented in the previous chapter, based on a reduced model replicating the real process of the additive building-up of the virole structure by means of LMD, provided a transient temperature field as a result. This transient temperature field was applied as a thermal load in an uncoupled thermo-mechanical analysis. For this calculation, an isotropic elastic–plastic material definition with temperature dependant mechanical values for the Young's modulus, yield stresses and strain hardening was implemented. Additionally the change of phase from powder into solidified material was considered by applying a phase change Leblond model in the finite element solver SYSWELD [19, 20]. Details of the used thermal and mechanical material properties are provided in Table 3 for a temperature range. The temperature dependent material properties of the solid (casted) IN718 were taken from the literature (Sysweld) [20]. The thermal material properties for IN718 powder were induced according to the work of Biceroglu et al. [21].

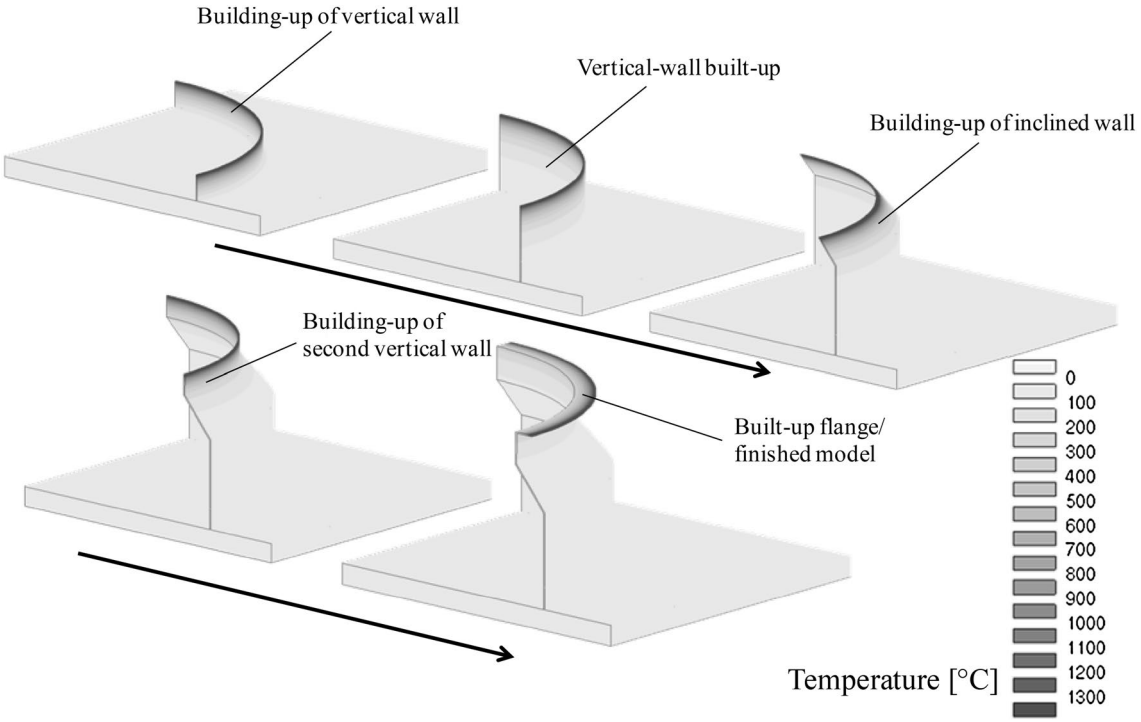

Fig. 5 Building-up process of the model and temperature field calculation during powder layer deposition in a layer-wise approach

Table 3 IN718 powder and solid material properties

Material properties	Powder		Solid material			Units
	20 °C	500 °C	20 °C	500 °C	800 °C	
Thermal						
Specific heat capacity	222	261	444	512	702	J/(kg·K)
Thermal conductivity	0.2	0.3	12.5	17.9	23.1	W/(m·K)
Density	4073	3930	8146	7979	7851	kg/m^3
Mechanical						
Young's modulus	–	–	210	181	140	GPa
Yield strength	–	–	700	493	376	GPa
Tensile strength	–	–	900	643	396	GPa
Poisson ratio	–	–	0.38	0.38	0.38	–
Thermal expansion	–	–	0	0.007	0.013	mm

First the shape distortions and residual stresses of the virole part while still attached on the base plate (i.e. prior to cut-off) were computed. Figure 6 illustrates the initial distortion results in the *x*-(radial) direction compared to 3D scanned geometries provided with the ATOS measuring equipment compared to the ideal CAD geometry. As it can be observed in Fig. 6 the FE model provides good results for the lower region of the virole part prior to cut-off with a deformation in the negative *x*-direction, i.e. reduction of the component radius of up to 1.2 mm while the measurements provide similar results with axial displacement in this area of up to more than 1.1 mm. The results continue to agree for the area of the inclined wall with no significant radial displacement for both the FE model and the scanned 3D geometries. However, in the upper vertical wall the FE model indicates an increase of the virole part radius of around 0.5 mm whilst the measurements show a reduction of the radius to around 0.4 mm. The FE model fails to provide sufficient distortion tendencies in this area of the part. The reason for these discrepancies lies in the fact that while the finite element geometry grows longer, i.e. powder layers are processed and added, the not yet deposited continuum, i.e. mesh, is displaced due to the already deformed underlying processed model. For this reason, a distortion with a wrong tendency can be initiated in this region, especially when interfering with the actual layer being processed in an

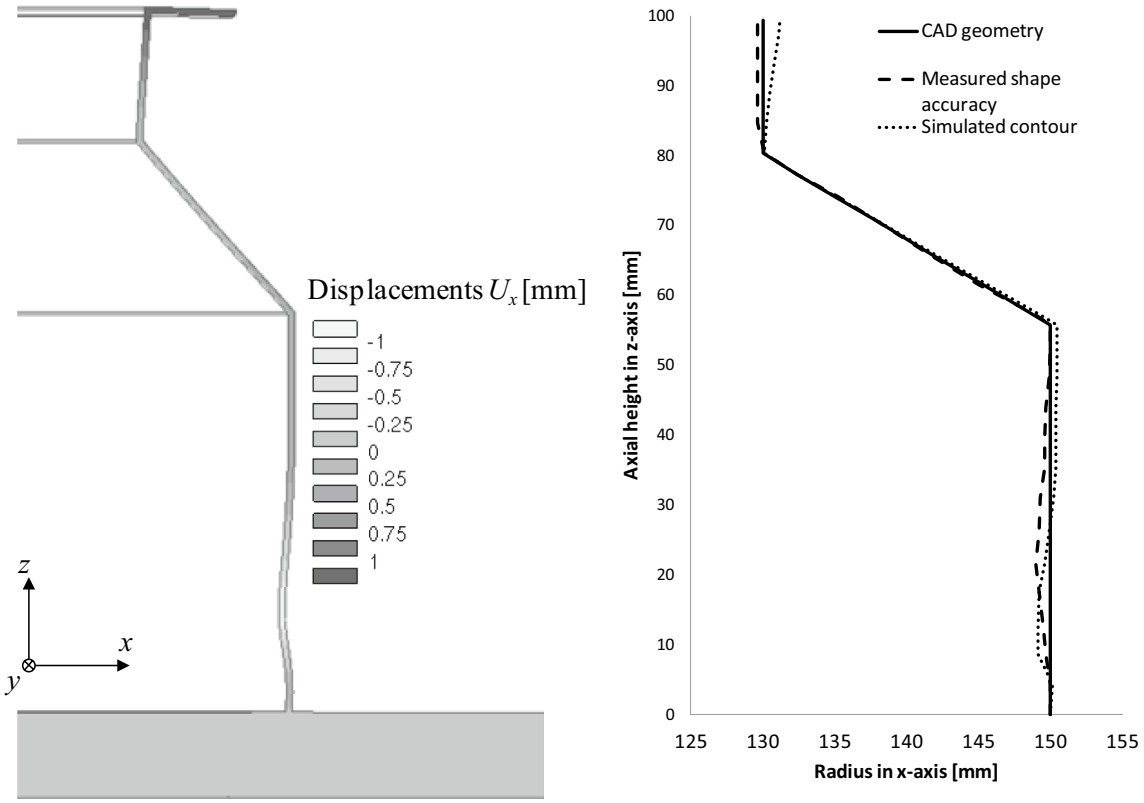

Fig. 6 Measured and simulated virole demonstrator component distortion results in *x*-(radial) direction prior to cut-off from substrate compared to target CAD geometry

already distorted mesh. On the contrary, in the real process performance, even though shape inaccuracies may occur due to thermal shrinkage during processing, the machine setup deposits each new powder layer in the exact CAD target position, therefore initiated shape distortions are compensated during the course of the build-up process.

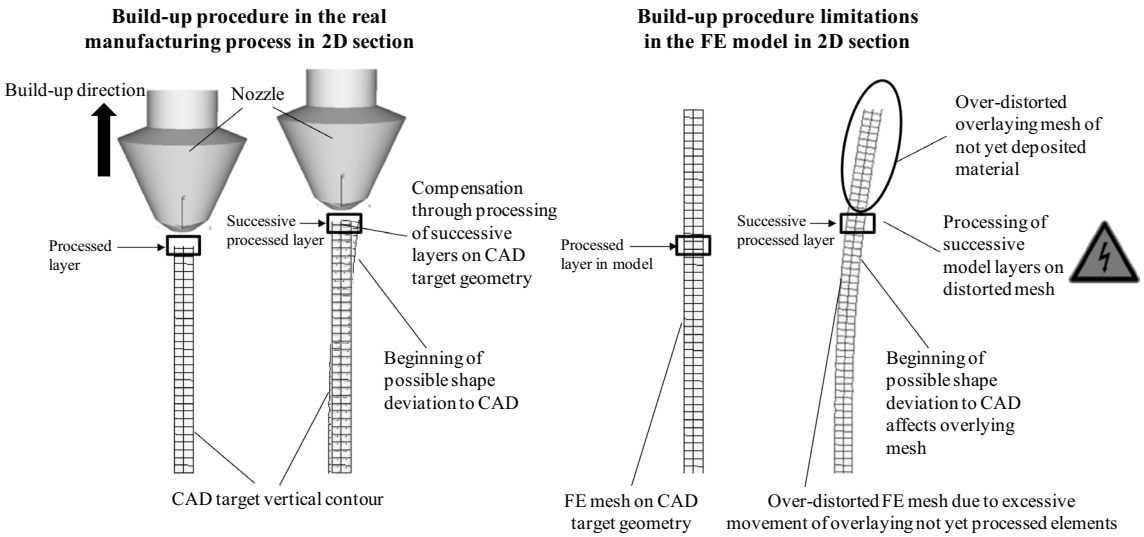

Fig. 7 Possible source of the shape accuracy discrepancy in the build-up procedure between simulation and experiment during the LMD processing of thin-walled components

Figure 7 visualises the difference between the model build-up procedure and the build-up procedure in the real manufacturing process.

Figure 8 presents the initial distortion results in the z-(axial/build-up) direction compared to 3D scanned axial shrinkage provided with the ATOS measuring equipment compared to the ideal CAD axial length. As far as the axial distortions prior to cut-off are concerned the overall shrinkage of the FE model proves to be in good agreement with the measurements. A total shrinkage of almost 1.4 mm is calculated by the FE model while the 3D scans provided an average total shrinkage of approximately 1.7 mm.

The finished virole part was subsequently cut-off at a height of approximately 12 mm from substrate. This substrate removal process step is also modelled in the simulation chain in a final "spring-back" calculation step (equilibrium after substrate removal) in order to calculate the final component shape. The average von Mises residual stress distribution prior and after cut-off in the virole part is demonstrated in Fig. 9. A significant alteration of the stress distribution is observed due to the cut-off operation, especially in the cut-off area, i.e. in the area where the component is attached to the base plate.

The final virole shape distortion results after cut-off from the substrate in the x-(radial) and z-(axial, build-up) direction, respectively, compared to 3D scans are shown in Figs. 10 and 11. As it can be observed in Fig. 10 the FE model provides a very good correlation with 3D scans in the lower region of the virole part after the cut-off operation from substrate with deformations in the negative

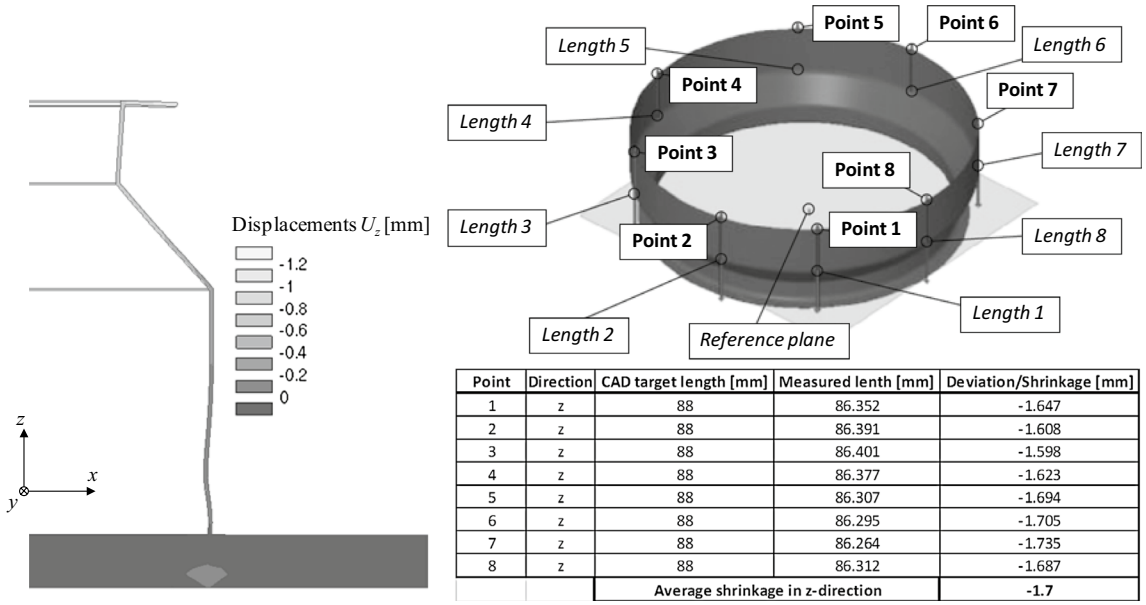

Point	Direction	CAD target length [mm]	Measured lenth [mm]	Deviation/Shrinkage [mm]
1	z	88	86.352	-1.647
2	z	88	86.391	-1.608
3	z	88	86.401	-1.598
4	z	88	86.377	-1.623
5	z	88	86.307	-1.694
6	z	88	86.295	-1.705
7	z	88	86.264	-1.735
8	z	88	86.312	-1.687
		Average shrinkage in z-direction		-1.7

Fig. 8 Virole demonstrator component distortion results in z-(axial, build-*up*) direction prior to cut-off

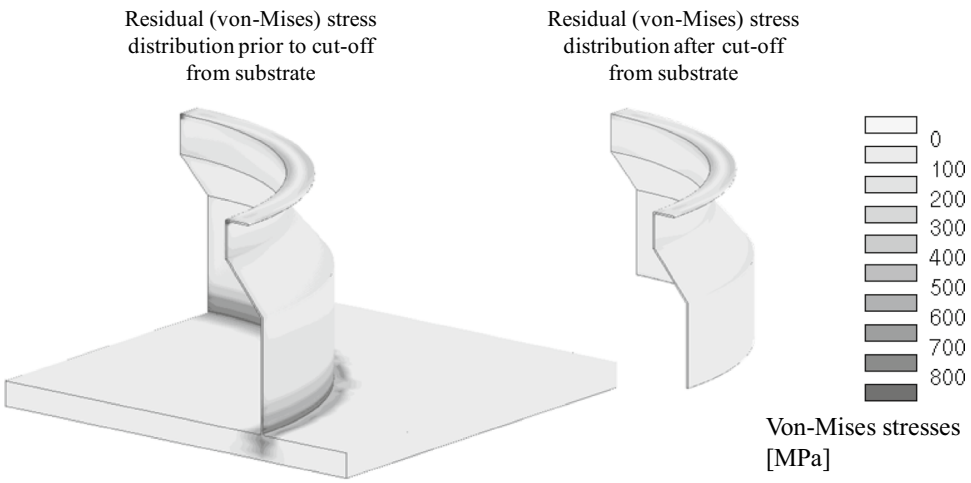

Fig. 9 Stress distribution after thermo-mechanical analysis while on substrate (*left*) and final stress relaxation after cut-off from base plate (*right*)

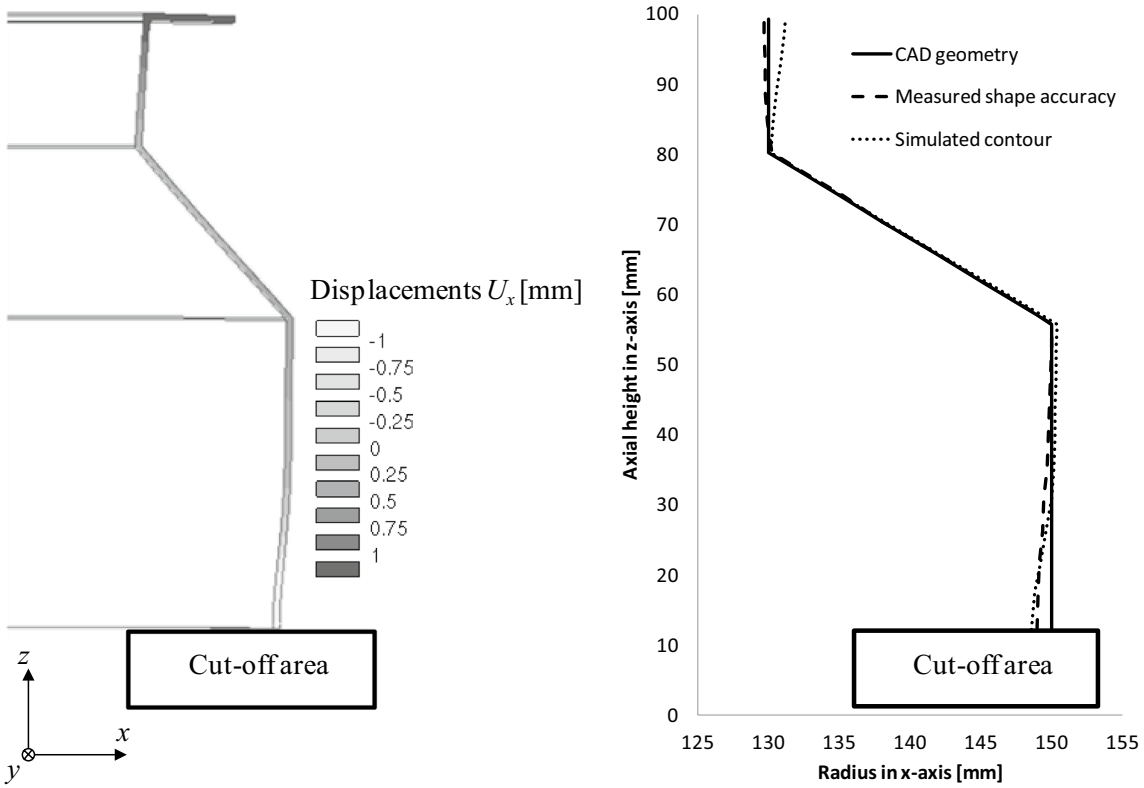

Fig. 10 Virole demonstrator component distortion results in *x*-(radial) direction after cut-off

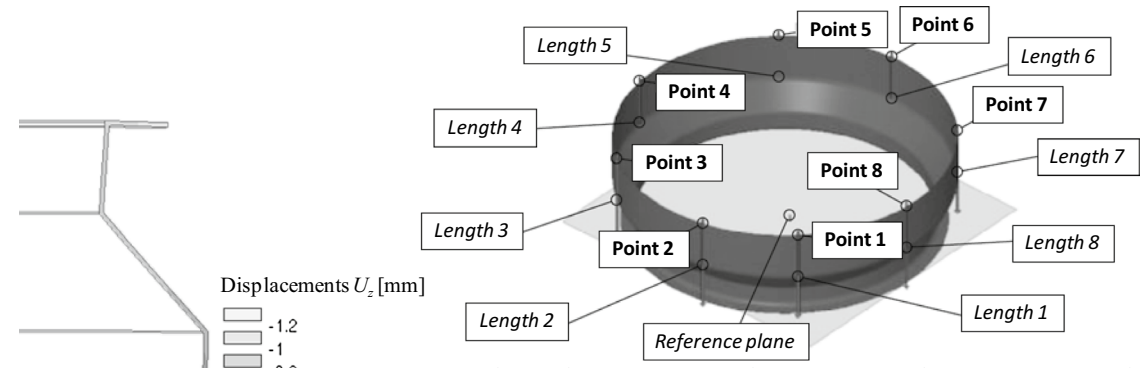

Point	Direction	CAD target length [mm]	Measured lenth [mm]	Deviation/Shrinkage [mm]
1	z	88	86.725	-1.273
2	z	88	86.786	-1.212
3	z	88	86.569	-1.43
4	z	88	86.38	-1.62
5	z	88	86.677	-1.323
6	z	88	86.706	-1.294
7	z	88	86.414	-1.586
8	z	88	86.39	-1.609
		Average shrinkage in z-direction		-1.4

Fig. 11 Virole demonstrator component distortion results in *z*-(axial, build-*up*) direction after cut-off

radial direction, i.e. reduction of the component radius of up to 1.2 mm. Simultaneously, the measurements demonstrate a comparable behaviour with a radius reduction of higher than 1.0 mm. The results continue to indicate a very good agreement for the area of the inclined wall with no significant radial changes for both the FE model

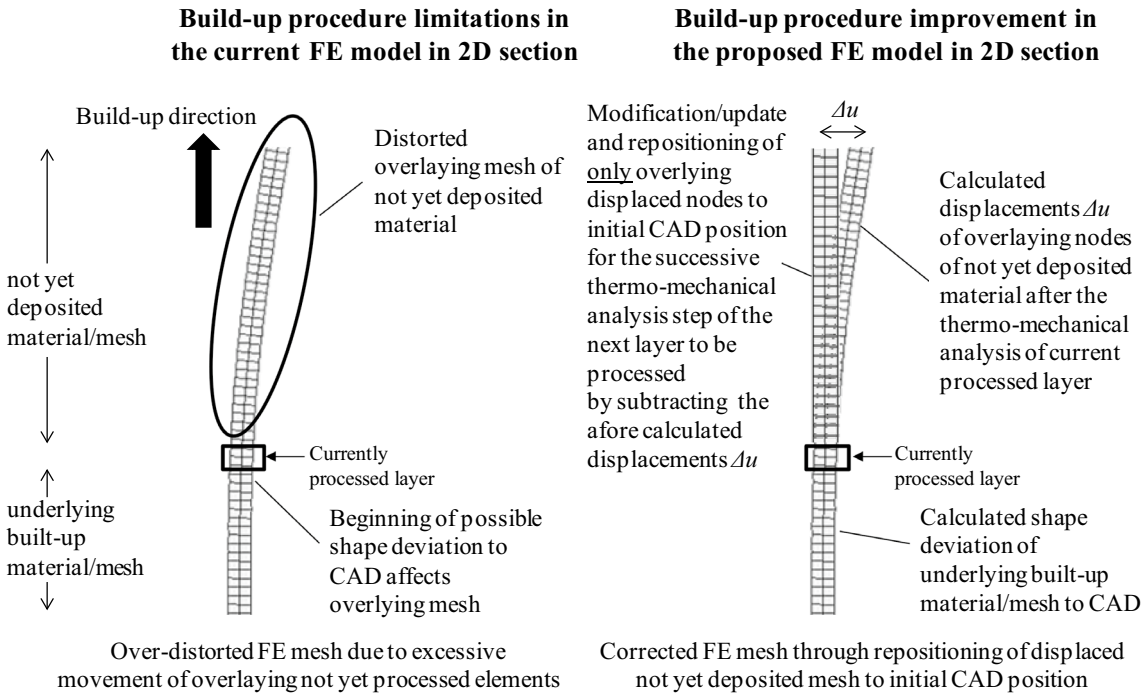

Fig. 12 Build-up procedure improvement through coordinate modification of the not yet deposited material to the initial CAD position after each simulation step

and the measured 3D scans. However, in the upper vertical wall the FE model fails to replicate the radial decrease and provides an increase of the radius of around 0.50 mm whilst the measurements show a reduction of the radius of around 0.35 mm. As far as the axial distortions after cut-off are concerned the overall shrinkage of the FE model is in a very good agreement with the 3D scans. A total shrinkage of approximately 1.2 mm is calculated by the FE model while the 3D scans provided a total average axial shrinkage of approximately 1.4 mm.

5 Discussion and outlook

In this paper a heat input reduction approach for LMD processing of a thin-walled virole aero-engine casing was presented. A reduced heat input temperature function based on real process parameters was developed and facilitated in a transient thermal simulation of the aero-engine demonstrator part. The key conclusion which can be drawn from the above findings are summarised as follows:

- The 3D scan measurements of the real virole component exhibit (Figs. 8, 11) that the axial variation along the components circumference after the cut-off process does not exceed ±2%, for both prior to cut-off and after cut-off geometries. Similarly, the radial measurement variation is limited to less than ±1%. These evidences lead to the conclusion that the continuous helicoid LMD processing of the laser does not create any significant asymmetry. This satisfies the assumption that symmetry conditions for modelling the components' geometry and a simultaneous heat source across the whole layer circumference for replicating the laser processing is acceptable.
- The computed deformed shape and residual stress distribution of the virole component proved similar tendencies as the experimental measurements, particularly after the support cutting, where the stress relaxation allocated the component's final geometry. Hereby, the FE model provides deformation discrepancy of less than 15% compared to the experimental 3D measurements in regions adjacent to the substrate, i.e. fixed supported, within a height of 80 mm from substrate including the area of the inclined wall. As the model grows longer along the model build-up direction, accumulated mesh deformations induced in the model layers produce an incorrect movement of the overlaying not yet deposited mesh. For this reason the computed shape accuracy in regions further away from the substrate, particularly in the region above the inclined wall higher than 80 mm from substrate, appear to accumulate the already occurred deformations in the underlying model and provide insufficient final shape results (Figs. 6, 8).

- After identifying this source of discrepancy in the shape accuracy prediction between the simulation and measurements of the demonstration component which is related to the mesh definition, the introduced modelling approach is planned to be investigated further with respect to its mesh accuracy. In this context the update of the deposited mesh in the thermo-mechanical simulation on the target CAD position, similar to real process, will be striven. Such a modelling approach can be realised with the aid of commands available in the finite element solver SYSWELD which allow for the modification of the node coordinates after each thermo-mechanical simulation step [20]. The calculated displacements Δu of merely the overlaying nodes, i.e. nodes above the processed layer, of the not yet deposited material after each thermo-mechanical analysis of currently processed layer will be modified, i.e. repositioned, to the initial CAD position with the aid of the subroutine *modify coordinates*. This operation will prepare the mesh for the successive thermo-mechanical analysis step of the next layer to be processed by subtracting the afore calculated displacements Δu similar to the corrective effect of the real CNC LMD process, in which the position of the last printed layer does not effect the position of the overlying following layer. This will prevent the incorrect movement of the overlying predefined mesh layers, which have not yet been processed, and, therefore, reduce undesirable accumulated shape distortions, due to a distorted positioning of the overlaying mesh during the model build-up procedure (Fig. 12).
- Finally, a simulation parameter sensitivity study of the manufactured component can be conducted in order to study the variation of the final computed shape compared to the experimental results. This will assist to evaluate the stability and reliability of the simulation approach for predicting the shape accuracy and the residual stresses in LMD processes. Specifically, modelling specific parameters as mesh thickness and equivalent load definition over model layer thickness can be varied in order to identify possible model limits and provide an outcome of the computational time reduction benefit versus the result accuracy. To this end, inverse engineering strategies can be applied in order to minimise shape deviations during LMD processing by utilising pre-distorted initial geometries, which will approach the ideal CAD shape even more accurately.

Acknowledgements The investigations and results presented in this paper were accomplished in the framework of the MERLIN Project which has received funding from the European Commission's 7th Framework Programme FP7 2007–2013 under the Grant agreement 266271. Project website: http://www.merlin-project.eu.

References

1. Ding D, Pan Z, Cuiuri D, Li H (2015) Wire-feed additive manufacturing of metal components: technologies, developments and future interests. Int J Adv Manuf Technol 81:465–481
2. Nowotny S, Scharek S, Beyer E, Richter KH (2007) Laser Beam Build-Up Welding: Precision in Repair, Surface Cladding, and Direct 3D Metal Deposition. J Therm Spray Technol 16:344–348
3. Zhang K, Shang XF, Liu WJ (2011) Laser metal deposition shaping system for direct fabrication of parts. Appl Mech Mater 66–68:2202–2207
4. Zhang A, Qi B, Shi B, Li D (2015) Effect of curvature radius on the residual stress of thin-walled parts in laser direct forming. Int J Adv Manuf Technol 79(1):81–88
5. Sridharan N, Chaudhary A, Nandwana P, Babu SS (2016) Texture evolution during laser direct metal deposition of Ti-6Al-4V. JOM 68(3):772–777
6. Khademzadeh S, Parvin N, Bariani PF (2015) Production of NiTi Alloy by direct metal deposition of mechanically alloyed powder mixtures. Int J Precis Eng Manuf 16(11):2333–2338
7. Mercelis P, Kruth JP (2006) Residual stresses in selective laser sintering and selective laser melting. Rap Prototyp J 12(5):254–265
8. Zaeh MF, Branner G (2010) Investigations on residual stresses and deformations in selective laser melting. Prod Eng 4(1):35–45
9. Ng GKL, Jarfors AEW, Bi G, Zheng HY (2009) Porosity formation and gas bubble retention in laser metal deposition. Appl Phys A 97:641–649
10. Tobar MJ, Amado JM, Lamas J, Yáñez A (2010) Effect of processing parameters in manufacturing of 3D parts through laser direct metal deposition. In: Proceeding 36th international MATADOR conference, Manchester, UK, 2010. Springer, London, pp 451–454
11. Mahamood RM, Akinlabi ET (2015) Processing parameters optimization for material deposition efficiency in laser metal deposited titanium alloy. Lasers Manuf Mater Process 3:9–21
12. Choi J, Chang Y (2006) Analysis of laser control effects for direct metal deposition process. J Mech Sci Technol 10(10):1680–1690
13. Song L, Bagavath-Singh V, Dutta B, Mazumder J (2012) Control of melt pool temperature and deposition height during direct metal deposition process. Int J Adv Manuf Technol 58:247–256
14. Song X, Xie M, Hofmann F, Illston T, Connolley T, Reinhard C, Atwood RC, Connor L, Drakopoulos M, Frampton L, Korsunsky AM (2015) Residual stresses and microstructure in powder bed direct laser deposition (PB DLD) samples. Int J Mater Form 8:245–254
15. Papadakis L, Loizou A, Risse J, Bremen S, Schrage J (2014) A computational reduction model for appraising structural effects in selective laser melting manufacturing. Virtual Phys Prototyp 9(1):17–25
16. Labudovic M, Hu D, Kovacevic R (2003) A three dimensional model for direct laser metal powder deposition and rapid prototyping. J Mater Sci 38(1):35–49
17. Zhu G, Zhang A, Li D, Tang Y, Tong Z, Lu Q (2011) Numerical simulation of thermal behavior during laser direct metal deposition. Int J Adv Manuf Technol 55(9):945–954
18. Radaj D (1992) Heat effects of welding. Springer, Berlin
19. Leblond JB (1984) A new kinetic model for anisothermal metallurgical transformations in steels including effect of austenite grain size. Acta Metall 32(1):137–146
20. SYSWELD (2006) Sysweld user's manual. ESI Group, Paris
21. Biceroglu O, Mujumdar AS, van Heiningen ARP, Douglas WJM (1976) Thermal conductivity of sintered metal powders at room temperature. Lett Heat Mass Transf 3:183–192